scientific reports

Check for updates

OPEN

Phosphorus transitions driven by cyclone biparjoy linked middle east North Africa (MENA) and Indian Thar Desert dust storm pathways in Asia's largest grassland

Rupak Dey[1]✉, Seema B. Sharma[1]✉, Mahesh G. Thakkar[2], Ranjit Kumar Sarangi[3], Abhiroop Chowdhury[4] & Aliya Naz[5]

Phosphorus (P) is an important nutrient for terrestrial ecosystems like grassland and plays a critical role in influencing primary productivity and hence ecosystem dynamics. The deposition of airborne dust, particularly from arid and semiarid regions, has been recognised as a significant source of phosphorus input in distant ecosystems. The study area, the Banni grassland, is a semiarid ecosystem with a unique geological history that has experienced degradation for various natural and anthropogenic reasons. It is located in the arid tract of western India. Soil samples were collected from 10 × 10 km grid locations in the grassland before, 48 h after, and 20 days after a cyclonic storm, Biparjoy, which hit the region in June 2023. Statistical analyses (Shapiro–Wilk normality and Kruskal–Wallis H test) were performed on the data to assess the differences in phosphorus concentrations in terms of PAC (Phosphorus Activation Coefficient) among the phases. To examine the long-range transport of dust-borne phosphorus and its subsequent deposition in the target grassland, we employed an interdisciplinary approach that integrated satellite imagery and ground-based measurements. Spatial and temporal variations in dust emissions were assessed using satellite remote sensing data, while ground truthing was performed for phosphorus content analysis using standard protocols. The aerosol data from MERRA-2 for the past 40 years were used to examine the relationships between aerosol concentrations and wind direction and speed. Our findings revealed that the Middle East, North Africa, and Thar Desert significantly contributed to phosphorus deposition in the target grassland during specific seasons. The SW cyclone 'Biparjoy', which followed the same track of aerosol loading (MENA), made landfall in this zone (June 16, 2023) and affected the P depositional patterns. The pre-cyclone, post-cyclone and 20 DAC (days after cyclone) had AP values of 15.15, 22.54 and 24.06, respectively. However, the TP values were 45.81 ± SE = 1.73, 60.95 ± SE = 1.39 and 61.98 ± SE = 1.40, respectively. The highest TP values were in phase 3 (20 DAC phase) (61.89 ± SE = 1.40). Similarly, the transformation of locked forms of P to bioavailable forms was coincidental with higher PSM (Phosphate Solubilising Microorganisms) in soil samples. Dust storms and other atmospheric circulation patterns were found to play pivotal roles in facilitating the long-range transport of phosphorus-laden dust particles from these source regions to the target grassland. Ultimately, our research contributes to the broader understanding of global nutrient cycling and land–air interactions, enabling informed decision-making for the conservation and sustainable management of terrestrial ecosystems.

Keywords Dust, Phosphorus, Grassland, Cyclone, Soil

[1]Department of Earth and Environmental Science, KSKV Kachchh University, Mundra Road, Bhuj, Kachchh, Gujarat 370001, India. [2]Birbal Sahni Institute of Palaeosciences, 53 University Road, Lucknow 226007, India. [3]Marine Ecosystem Division, Space Applications Centre(ISRO), Ahmedabad, India. [4]Jindal School of Environment and Sustainability, O.P. Jindal Global University, Sonipat, Haryana, India. [5]Jindal School of Liberal Arts and Humanities, O.P. Jindal Global University, Sonipat, Haryana, India. ✉email: rupak.2404@gmail.com; seemabhargavsharma@gmail.com

Grasslands, one of the world's largest terrestrial ecosystems due to their size (excluding Greenland and Antarctica), cover approximately 40.5% of the planet's terrestrial surface and are a vital land use type for supplying food and attaining the Sustainable Development Goals of the United Nations[1,2]. Grasslands play a significant role in controlling temperature and soil conservation in addition to making a significant contribution to the global carbon cycle[3]. These ecosystems are essential for sustaining biodiversity, carbon sequestration, and providing basic ecosystem services. Despite their significance, grasslands are undergoing rapid and widespread degradation across many parts of the world, with nearly 49% of global grassland areas affected to some extent[4–6]. Grassland ecosystems are generally recognized as being nutrient-limited, and numerous studies have identified nitrogen and phosphorus as the principal nutrients restricting their productivity[7–10]. Phosphorus ranks as the second most important limiting factor in grassland ecosystems, after nitrogen[11]. Phosphorus is essential for life on Earth, and several biogeochemical processes influence how it is distributed in terrestrial and marine ecosystems[12]. The primary source of phosphorus in any soil system is the weathering of parent rock with a phosphatic composition and is primarily found in the hydrosphere and lithosphere[13]. Parent material encompasses not only the original bedrock but also secondary deposits such as alluvial, aeolian, and colluvial sediments[14]. Studies involving global modelling indicate that more than 82% of the world's P emissions (1.4 Tg P yr^{-1}) originate from desert dust, which is a significant source of P[15]. The atmospheric deposition of mineral aerosol dust can serve as a significant source of nutrients, including phosphorus (P), for terrestrial ecosystems[12,16]. Dust-borne phosphorus can account for a substantial portion of the soil's phosphorus budget[17,18], and in some regions, it may play a crucial role in regulating ecosystem productivity[19]. The transport of atmospheric total phosphorus (TP) differs fundamentally from nitrogen, as phosphorus lacks a stable gaseous phase in the Earth's atmosphere. As a result, TP is predominantly confined to aerosols[15,20]. It enters the atmosphere as dust and then gets deposited or removed by aerosol aggregation with falling raindrops and recent studies have highlighted aerosols as significant sources of total phosphorus[21–25]. The biggest dilemma that turnsout to be the real game changer in P dynamics of soil is its 'Bioavailability'[26]. Soils with high total P content can still cause Available Phosphorus (AP) deficiencies in crops because much of the P becomes immobilized or 'fixed' by Fe and Al ions in acidic soils, and by Ca and Mg ions in alkaline soils[27,28]. This fixation process impacts not only the natural phosphorus present in the soil but also the phosphorus added through chemical fertilizers[13]. However, a more thorough list of emissions also includes dust from soils, the movement of sea salt, volcanic eruptions, biogenic sources, and the burning of fossil fuels, biofuels, and biomass[22,29]. The mineral dust produced when soils are eroded by wind and the P emissions caused by combustion are the two main sources of phosphorus in the atmosphere worldwide[30,31]. Numerous studies worldwide have documented dust deposition as a significant source of phosphorus, enriching ecosystems and acting as a natural fertilizer[16,32–38]. These particles eventually settle on land through both wet and dry deposition, delivering phosphorus to ecosystems[16,39,40]. Atmospheric phosphorus fertilises plants and contributes to Earth's biogeochemical phosphorus cycle[31]. Through the biogeochemical interactions of macro- and micronutrients that feed seas and continents, mineral dust contributes significantly to both the climate system and the maintenance of ecosystems[32]. The main worldwide dust sources are dry and semiarid areas, where particles may be lifted into the atmosphere and deposited far from their sources[41]. Sand and dust storms (SDSs) are significant severe meteorological occurrences that occur in dry regions when dust particles are carried by turbulent winds[42,43]. These lower atmospheric meteorological occurrences have an impact on the environment, and in recent years, their importance has grown in relation to climate, human health, and socioeconomic factors[44]. The dust cycle plays an important role in terrestrial ecosystems[16,33].

Currently, dry soil is exposed to strong winds during specific periods of the year, which is why subtropical desert areas, semiarid regions, and semihumid regions are the main sources of dust generation[45–47]. In particular, dry and semiarid deserts that stretch from West Africa to northern China make up the majority of the world's dust-producing regions in the Northern Hemisphere[48]. The most dust-prone regions in the globe are those in the Middle East and North Africa (MENA)[47,49–52]. Because of the predominant westerly wind in the premonsoon season, dust storms that originate in Africa's Sahara Desert, Arabia, the Middle East, Afghanistan, and the Thar Desert regions are carried by the wind to the Indo-Gangetic Plains and the Himalayas[53–55] via the west Indian tract that encompasses the Banni grassland. When these dust storms are entrained into the atmosphere and transported by dominant wind patterns over long distances, they finally descend onto the surface, causing phosphorus deposition in grasslands. The nutrient balance and general ecosystem health of receiving grassland regions might be affected by the deposition of phosphorus via this long-range atmospheric route.

Studies suggest that climate change may cause the Thar Desert to become greener by the century's end, as rainfall in semi-arid areas has surged by 1050% from 1901 to 2015[56]. Analysis of weather data shows that the Indian monsoon is shifting westward, which could result in a 25% rise in rainfall in the northwest and west, alongside a 10% decrease in the northeast[56]. This uptick in precipitation has the potential to enhance agricultural productivity considerably, reshaping the socio-economic dynamics of the region. Strong seasonal and aerosol variations across India from year to year are mainly caused by the regional monsoon system, atmospheric dynamics, seasonally varying air mass patterns, and spatiotemporal distributions of emission sources/sinks[57,58]. Because of the Indian summer monsoon and its accompanying vertical wind shear, which effectively prevents large storms from developing while sea surface temperatures (SSTs) are at their highest, the majority of storms in the Arabian Sea tend to be small and dissipate quickly[59]. However, over the last 30 years, a shift in the wind circulation pattern over the northern Arabian Sea has allowed for the formation of larger storms[60]. As a result, violent cyclonic storms have become more common in recent years in the Saurashtra and Kachchh areas of the northwest coast of India[61]. Recent increases in anthropogenic aerosols have increased storm severity over the Arabian Sea[62].

Biparjoy, a cyclonic storm, formed in the Arabian Sea. Biparjoy, which became a cyclonic storm on June 6, 2023 pounded the Kutch shore for more than ten days. This has made it one of the most powerful cyclones to hit India in recent decades because of its peak intensity, with a maximum of 3 min of sustained winds of 165 km/

hr. The storm made landfall (June 16, 2023) at Naliya (95 km/hr) before moving on through the Banni grassland and last, to the outskirts of Rajasthan state in India. Severe rainfall and high winds occurred in Gujarat's coastal areas, causing significant damage in the districts of Kutch and Rajkot.

Phosphorus applied as an external input gets locked in forms that are unavailable to the plant roots. Certain specialised microorganisms PSM (Phosphate Solubilising Microorganisms) have the ability to transform this locked form to bioavailable forms through complex solubilisation and mineralisation of inorganic and organic P respectively[28]. The soil pH plays a major role in comprehending the forms of P that would be either locked or available. The cyclonic dust storm besides being a source of P deposition, could possibly alter the soil chemistry in a way to render availability of P to the plants. This is perhaps attributable to the PSM that flourish in the conducive environment created. The present study is a maiden attempt to understand how P chemistry that has long been understood to be altered by inherent factors of micro ecological zone, could also be affected by the external large scale factors as cyclones that in conjugation with dust storms contribute to PAC (Phosphorus Activation Coefficient), ratio of the Available Phosphorus (AP) to Total Phosphorus (TP) range suitable for the growth of grasses that are more sensitive to P dynamics then other terrestrial vegetation[63]. For the rational management of P in soil, both the amount and chemical form play an important role[26].

In conjunction with the cyclonic-driven aerosol movement, this study examines the significance of dust storms from the MENA and Thar Deserts as possible gamechangers in determining the pattern of phosphorus deposition in grassland ecosystems. The dust from these dry areas has the capacity to transfer phosphorus across continental distances and may have a large impact on nutrient dynamics in grassland environments. For successful ecosystem management and conservation efforts, it is essential to comprehend how dust storms from the Thar and MENA Deserts affect the patterns of phosphorus deposition in grasslands. This study will shed light on the relationship between distant dry areas and grassland nutrient dynamics, which will help us understand how ecosystems are interrelated across continents.

Materials and methods

Study area and geological setting

The Banni plains are among the most enigmatic geological features in the Kachchh region, Western India (23° 19′ to 23° 52′ N latitude and 68° 56′ to 70° 32′ E longitude) (Fig. 1). It is a highly semiarid fragile ecosystem that spans a large tract of approximately 3800 sq. km of slightly undulating and sloped terrain. Banni plains are predominantly flat saline lands with several shallow depressions that act as seasonal wetlands after monsoons, and during winters, they convert into sedge mixed grasslands, which are ideal dual ecosystems. The unique geology and tectonic behaviour of the Banni grassland watershed affect the nutrient distribution in the terrain. It was first declared a protected forest in May 1955 under the Indian Forest Act, 1927. However, over time, the grassland has deteriorated. The productivity of grasslands decreased from 4000 kg/hectare in the 1960s to 620 kg/hectare in 1999[64]. The area covered by grassland decreased from 142,000 hectares in 1989 to 63,000 hectares in 2009, while the area invaded by Prosopis juliflora expanded to 82,000 hectares[65]. The area experiences significant fluctuations in annual rainfall in the Indian Summer Monsoon (ISM) region, which is approximately 317 mm on average and is erratic and low (mean 288 mm), with a coefficient of variationbetween60 and 80%[66,67]. The monsoon season, which lasts from June to September, brings more than 80% of the annual precipitation. The average temperature of Banni varies from 49 °C in the summer (May–June) to 10 °C in the winter (January-February)[66]. The region now exhibits significant levels of soil salinity, recurrent drought occurrences, and strong yearly seasonality[68]. The Kachchh area offers outstanding representations of tectonically influenced landscapes, where the landforms are the results of earth movements along tectonic lineaments of the Pre-Mesozoic basin architecture that were created by the primordial fault pattern in the Precambrian bedrock and have evolved essentially as a result of several phases of tectonic movements since the Late Jurassic[69–71]. As a consequences of such movement higher mean surfaces occur in Bhirandiara- Bhojardo area[67]. The geomorphology reveals that the Banni Plains are a large palaeo mudflat with an elevation of 2–12 m above mean sea level. There are many ephemeral streams, viz. Nara, Chari, Kadrai, Bhukhi, Nirona, Kaila, Pur, Kasvali, Lotia and Khirsara that flow across the Kachchh Mainland Fault (KMF) and into the Banni Plains from the south. These ephemeral rivers deposited alluvial fan sediments, which cover the southern end of the Banni plains. The Banni Plain used to be one of the finest grasslands in Asia known as the 'Banni Grassland Reserve', which has been reduced to a remnant one due to its rapid degradation.

Soil sampling and analysis

Soil surveys and field data were collected from the arid grasslands of Banni and its fringes. In total, 45locations were used for the investigation; these locations were established during 3 phases: premonsoon (i.e., pre cyclone Biparjoy), post cyclone and 20 days after cyclone (DAC). The coordinates and altitudes of the research locations were recorded on-site using a portable Garmin 72 H Global Positioning System. The survey locations had a bio-climate that ranged from arid to hyperarid. We used ArcGIS 10.7 to incorporate a 10×10 km (Fig. 2) remote sensing grid and transects at each research location with a subgrid of approximately 5×5 km to gather soil samples down to a depth of 30 cm. The sampling locations were selected from all elevations of the research region to reduce the possible impacts of various microclimates influenced by slope, aspect, and tectonics. The physical and chemical properties of the soils were analysed according to standardised standard protocols, as explained by Alef&Nannipieri[72]. For available phosphorus, Olsen's method for neutral alkaline soil[73] was adopted. The total P in the soil samples was extracted by a mixture of concentrated sulfuric acid, hydrofluoric acid and hydrogen peroxide[74,] and the P concentration of the extract was determined using the same method as for available P. Soil organic carbon (SOC) and organic matter (OM) were determined using the titrimetric determination[75] method.

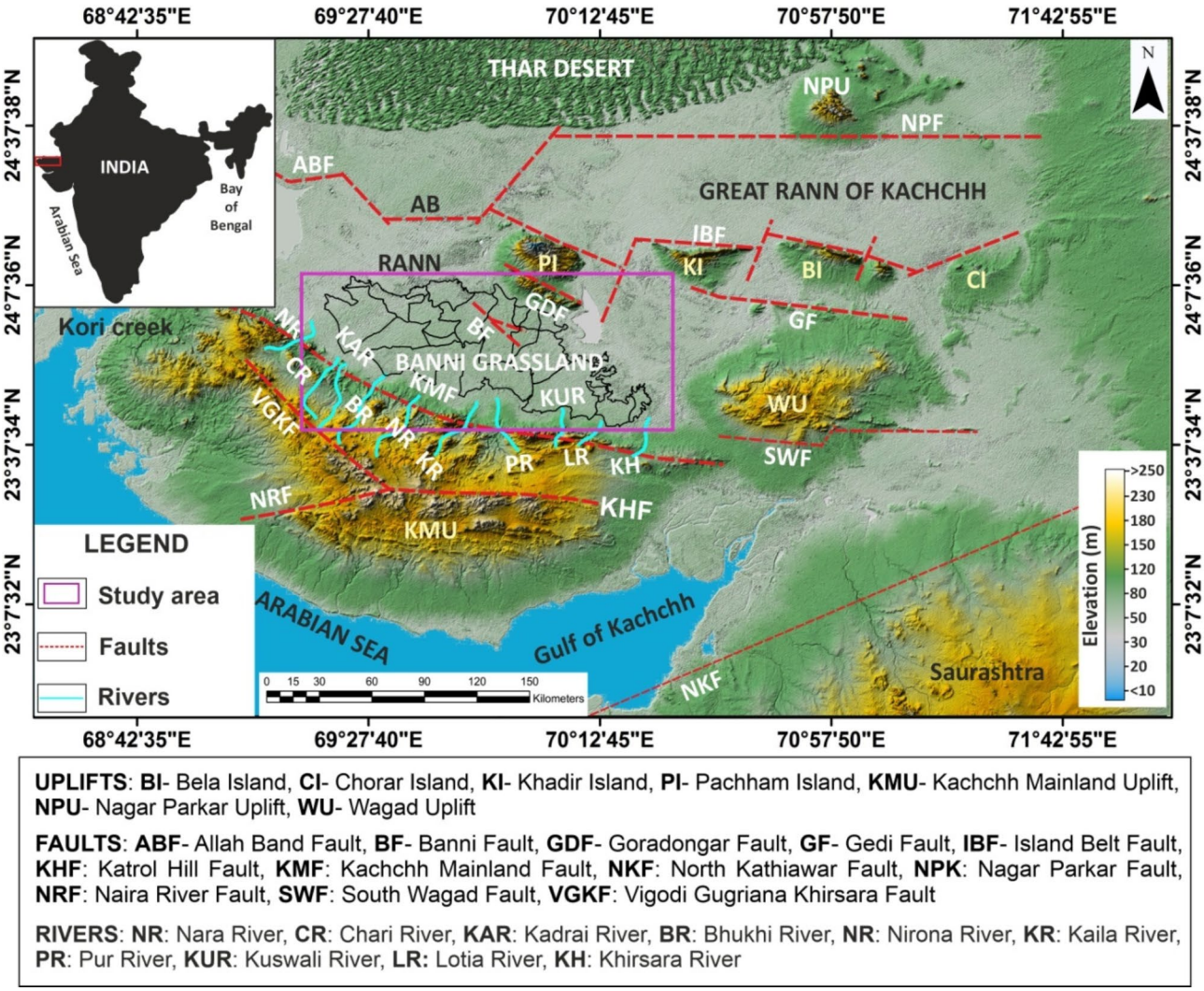

UPLIFTS: **BI**- Bela Island, **CI**- Chorar Island, **KI**- Khadir Island, **PI**- Pachham Island, **KMU**- Kachchh Mainland Uplift, **NPU**- Nagar Parkar Uplift, **WU**- Wagad Uplift

FAULTS: **ABF**- Allah Band Fault, **BF**- Banni Fault, **GDF**- Goradongar Fault, **GF**- Gedi Fault, **IBF**- Island Belt Fault, **KHF**: Katrol Hill Fault, **KMF**: Kachchh Mainland Fault, **NKF**: North Kathiawar Fault, **NPK**: Nagar Parkar Fault, **NRF**: Naira River Fault, **SWF**: South Wagad Fault, **VGKF**: Vigodi Gugriana Khirsara Fault

RIVERS: **NR**: Nara River, **CR**: Chari River, **KAR**: Kadrai River, **BR**: Bhukhi River, **NR**: Nirona River, **KR**: Kaila River, **PR**: Pur River, **KUR**: Kuswali River, **LR:** Lotia River, **KH**: Khirsara River

Fig. 1. Morphotectonic map of the study area displaying the primary ephemeral streams flowing northward into the Banni region. This map was created by the authors using Global Mapper software 24.1 (https://www.bluemarblegeo.com/global-mapper-download/) and Corel DRAW X8 (https://www.coreldraw.com/en/pages/coreldrawx8/).

For aerosols, we used data from the MERRA-2 (1981 January to 2021 December) and NASA Giovanni websites (https://giovanni.gsfc.nasa.gov/giovanni/). Accessing and analysing a wide variety of remote sensing data types is made available by the NASA Giovanni data analysis system. The MERRA dataset was replaced by MERRA-2 data by integrating improvements to the assimilation mechanism. Utilising the global positioning system enables the integration of contemporary hyperspectral radiance and microwave data with the GPS-Radio Occultation. These reanalysis products are produced by MERRA-2 using the GEOS-5 atmospheric model and data assimilation system version 5.12.4. The same spatial resolution (approximately 50 km in the latitudinal direction) as MERRA's global assimilation system is used to combine meteorological and aerosol information. The current analysis utilises monthly mean data from MERRA-2 for the 40-year period between 1981 and 2021 for (i) total aerosol scattering, (ii) dust wet deposition, and (iv) dust dry deposition at a spatial resolution of 0.5° × 0.625°. We also used wind direction and wind speed data from the NASA data access viewer website (https://power.larc.nasa.gov/data-access-viewer/) to determine the relationships between total aerosol scattering (TAS), dust wet deposition (DWD) and dust dry deposition (DDD) and between wind direction and wind speed. The total aerosol scattering of MERRA-2 was utilised for the period from 1981 to 2021 to estimate the climatology of aerosol scattering over the Banni grassland and nearby regions.

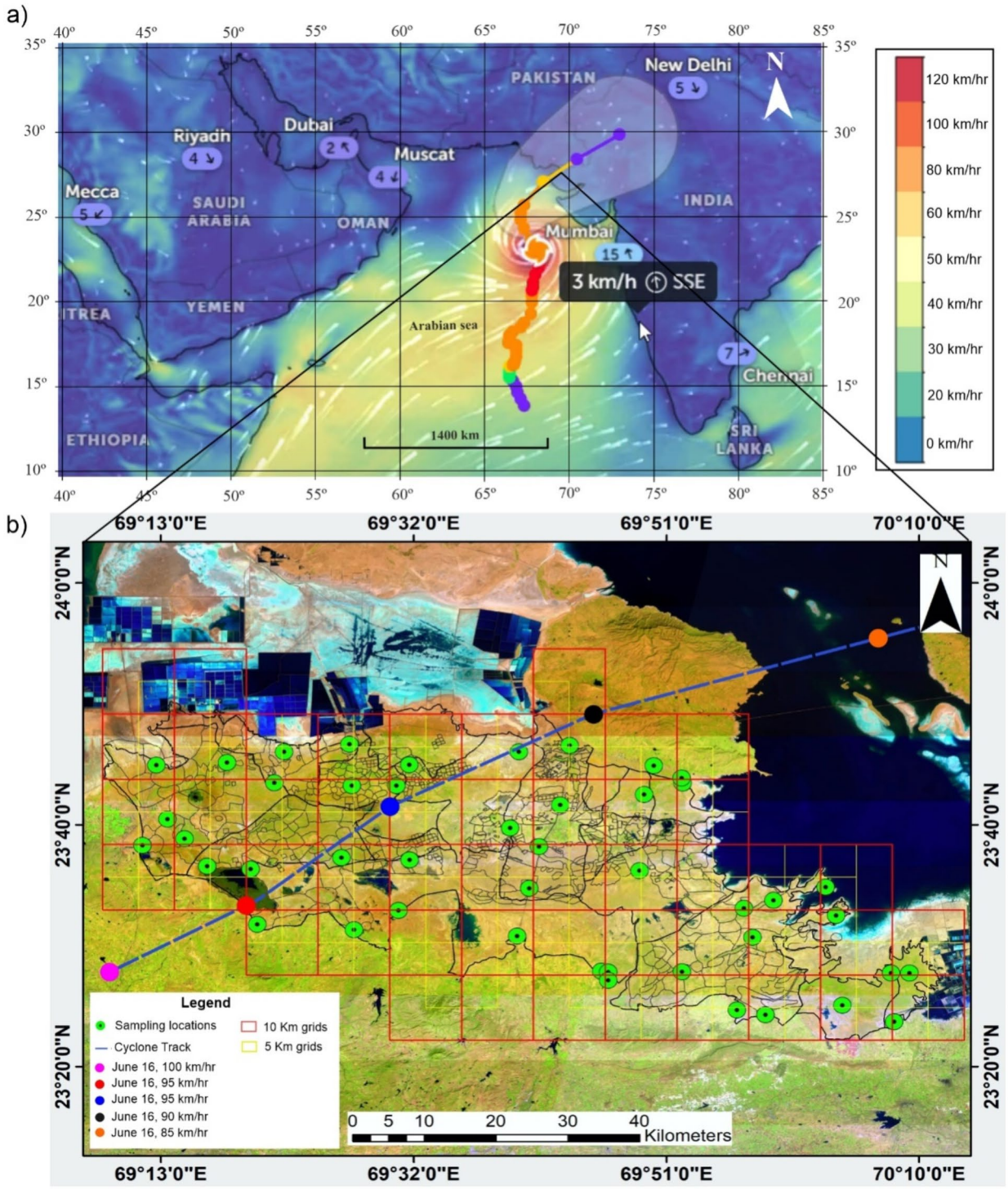

Fig. 2. (**a**) Showing the impacted area of cyclone Biparjoy; (**b**) Sampling strategy and locations with respect to the cyclone track. This map was created by the authors using ArcGIS software (version 10.7) (https://desktop.arcgis.com/en/system- requirements/10.7/arcgis-desktop-system-requirements.htm), Corel DRAW X8 (https://www.coreldraw.com/en/pages/coreldrawx8/) and Zoom Earth (https://zoom.earth/storms/biparjoy-2023/).

Statistical analysis

The datasets obtained from the above analysis were subjected to various statistical tests to determine the significant/non-significant differences in the concentrations of P and soil physicochemical parameters across various divisions of the Banni Grassland and surrounding fringes. First, the datasets were subjected to the Shapiro–Wilk normality ($p \leq 0.05$) test, which confirmed that the datasets were not normally distributed. Furthermore, the Kruskal–Wallis H test was chosen as the nonparametric test for determining significant

Tests of normality						
	Kolmogorov-Smirnov[a]			Shapiro–Wilk		
	Statistic	df	Sig.	Statistic	df	Sig.
pH	0.113	351	0.000	0.965	351	0.000
Soil Organic Carbon (%)	0.112	351	0.000	0.945	351	0.000
Available P (kg/ha)	0.082	351	0.000	0.958	351	0.000
Total P(kg/ha)	0.078	351	0.000	0.971	351	0.000
PSM (cfu/gm)	0.065	351	0.000	0.965	351	0.000
PAC (AP/TP)	0.072	351	0.000	0.932	351	0.000

Table 1. Tests of normality overall. [a]Lilliefors Significance Correction

Descriptive statistics							
	N	Range	Minimum	Maximum	Mean		Std. Deviation
	Statistic	Statistic	Statistic	Statistic	Statistic	Std. Error	Statistic
pH	351	1.66	7.12	8.78	8.0366	0.02032	0.38070
Soil Organic Carbon (%)	351	1.20	0.09	1.29	0.7581	0.01552	0.29083
Available P (kg/ha)	351	62.24	1.56	63.80	21.5855	0.71065	13.31401
Total P(kg/ha)	351	75.00	14.00	89.00	56.2507	0.95949	17.97601
PSM (cfu/gm)	351	7.72	0.00	8.62	2.2356	0.96	0.27
PAC (AP/TP)	351	1.65	0.05	1.72	0.38	0.01	0.04
Valid N (listwise)	351						

Table 2. Overall descriptive statistics of the parameters.

differences between various phases, viz., pre cyclone, post cyclone and 20th DAC. The significance level (α) was fixed at 5%. The following statistical software was used to carry out variousanalytical procedures: SPSS version 26 (IBM), SAS version 9.3, Microsoft Excel version 7, and Originpro 2022.

The present study examined the status of P deposition via aerosols using the satellite and ground data. The initial plan for the study was to set up the dust collection towers in the study area. However, as Indian Meteorological Department (IMD) radar data, Bhuj indicated a cyclone formation in the Arabian sea during the sample collection time. Hence, the plan was changed to track the cyclonic movement driven aerosols deposition that concurrently followed the same path of our study area (Fig. 2a, b).

Results and discussion

Statistical analysis of soil parameters

The Shapiro–Wilk test revealed that the datasets were not normally distributed ($p \leq 0.05$) (Table 1). Furthermore, the Kruskal–Wallis H test was selected as a nonparametric test that could be used to identify significant differences across means. Descriptive statistical tests were run on datasets (Table 2) obtained from all sampling locations across the 3 phases. pH, soil organic carbon (SOC), available phosphorus (AP), and total phosphorus (TP) had mean values of 8.03 ± SE = 0.02, 0.75 ± SE = 0.01, 21.58 ± SE = 0.71and 56.25 ± SE = 0.91, respectively.

Phase-wise variations in phosphorus levels and the influence of PSM

After splitting the data phasewise, descriptive statistics were calculated for the mean values and ranges (Table 3). The pre- cyclone, post- cyclone and 20 DAC (days after cyclone) had AP values of 15.15, 22.54 and 24.06, respectively. However, the TP concentrations were 45.81 ± SE = 1.73, 60.95 ± SE = 1.39and 61.98 ± SE = 1.40, respectively. The highest TP values were in phase 3 (20 DAC phase) (61.89 ± SE = 1.40). The value of PAC forpre- cyclone, post- cyclone and 20 DAC (days after cyclone) was 0.33 ± SE = 0.05, 0.38 ± SE = 0.03, 0.39SE = 0.04.

However, no significant difference was detected in the SOC values (H (2) = 3.52; $p > 0.05$). As an alternative to the post hoc test, a pairwise comparison was carried out to further determine which pair of datasets had significantly different values (Tables 6 and 7). For AP, phase 3 was significantly different from phases 1 and 2. However, phases 1 and 2 did not have significantly different mean values. For total P, phase 1 was significantly different from phases 2 and 3 (Fig. 3). However, 2 and 3 did not have significantly different values. Figure 4 shows the spatial interpolation maps of AP and TP across the three different phases.

The higher values of PSM were observed in phase 3 (2.04 cfu/gm) which concludes that the prolific growth of PSM occurred post cyclonic showers and this led to conversion of locked P forms to bioavailable P and hence an increase in AP was observed.

Descriptive Statistics								
Phase		N	Range	Minimum	Maximum	Mean		Std. Deviation
		Statistic	Statistic	Statistic	Statistic	Statistic	Std. Error	Statistic
1.00 (Precyclone)	pH	117	1.56	7.22	8.78	8.0862	0.03422	0.37017
	Soil Organic Carbon (%)	117	1.18	0.09	1.27	0.7221	0.02658	0.28752
	Available P (kg/ha)	117	56.34	1.56	57.90	15.1548	1.16361	12.58634
	Total P(kg/ha)	117	72.00	14.00	86.00	45.8120	1.73591	18.77679
	PSM (cfu/gm)	117	0.96	1.10	1.19	1.07	0.08	0.005
	PAC (AP/TP)	117	0.50	0.04	0.78	0.33	0.05	0.03
	Valid N (listwise)	117						
2.00 (Post cyclone)	pH	117	1.55	7.12	8.67	8.0118	0.03560	0.38506
	Soil Organic Carbon (%)	117	1.17	0.12	1.29	0.7761	0.02700	0.29203
	Available P (kg/ha)	117	57.13	1.67	58.80	22.5406	1.18469	12.81434
	Total P(kg/ha)	117	60.00	27.00	87.00	60.9573	1.39244	15.06159
	PSM (cfu/gm)	117	1.67	1.11	1.96	1.74	0.05	0.03
	PAC (AP/TP)	117	1.18	0.07	1.11	0.38	0.03	0.02
	Valid N (listwise)	117						
3.00 20 DAC (days after cyclone))	pH	117	1.55	7.12	8.67	8.0118	0.03560	0.38506
	Soil Organic Carbon (%)	117	1.17	0.12	1.29	0.7761	0.02700	0.29203
	Available P (kg/ha)	117	61.46	2.34	63.80	24.0612	1.31680	14.24338
	Total P(kg/ha)	117	61.00	28.00	89.00	61.9829	1.40260	15.17142
	PSM (cfu/gm)	117	1.67	1.24	2.04	1.92	0.02	0.04
	PAC (AP/TP)	117	1.72	0.12	1.22	0.39	0.04	0.05
	Valid N (listwise)	117						

Table 3. Phase wise descriptive statistics for the pre cyclone (phase 1), post cyclone (phase 2) and 20 DAC (days after cyclone) (phase 3) periods. Furthermore, the Kruskal–Wallis H test showed that there was a statistically significant difference in the AP ($H(2) = 6.84$; $p \leq 0.05$) and TP ($H(2) = 53.33$; $p \leq 0.05$) values across phases (Table 4). Mean Rank across phases is shown in Table 5.

Test Statistics[a, b]				
	pH	SOC	Available P (kg/ha)	TP
Kruskal–Wallis H	2.927	3.528	6.843	53.337
df	2	2	2	2
Asymp. Sig.	0.231	0.171	0.033	0.000

Table 4. Kruskal–Wallis H statistics across 3 phases of sampling. [a]Kruskal–Wallis Test [b]Grouping Variable: Time

Aerosol concentrations and spatial distribution patterns

The aerosol analysis data reveal distinct colours representing the variations in aerosol concentrations across the Kachchh area flowing from MENA (Fig. 5). Figure 6a shows that aerosol scattering increases from south to the northern regions, builds up near the Pachham island (an island just above the Banni Grassland), and continues farther north in the adjoining state of Rajasthan's Thar Desert. Additionally, the geographical distribution of dust aerosol scattering heterogeneity in the Kachchh region was demonstrated.

Aerosol movement driven by cyclonic influence has the potential to alter P transitions in grassland ecosystems of unique Asiatic grasslands in Banni. From 1981 to 2021, a spatial time average map of total aerosol scattering (TAS) of 550 nm monthly (Fig. 6a) and the monthly mean dust dry deposition over the Banni grassland and adjacent areas were retrieved from MERRA-2. In contrast to other portions of Kachchh (orange to light pink), the Banni region (dark brown) has areas of significant dust dry deposition (Fig. 6b). This indicates that although other areas of the study area have the lowest concentration of dust dry deposition (6.54 to 12.06 kg m^{-2} s^{-1}), north western and central Banni have the highest dust dry deposition. A similar assessment was made based on the monthly mean dust wet deposition (Fig. 6c) across the Banni grassland and its surroundings. The banni region (light pink) in this image displays areas with less wet deposition of dust than other sections in Kachchh (orange to light pink). This indicates that although other areas in Kachchh have greater concentrations of dust wet deposition (6.15 to 13.33 kg m^{-2} s^{-1}), western, central, and eastern Banni are experiencing the lowest levels of dust wet deposition. The monthly temporal average wind speed map (Fig. 6d), which shows the average wind speed throughout the years from 1981 to 2021, was utilised as a representation of dust aerosol loading. The light

Ranks			
Parameters	**Phases**	**N**	**Mean Rank**
pH	1.00	117	189.10
	2.00	117	169.45
	3.00	117	169.45
	Total	351	
SOC	1.00	117	161.62
	2.00	117	183.19
	3.00	117	183.19
	Total	351	
Available P (kg/ha)	1.00	117	164.13
	2.00	117	167.95
	3.00	117	195.91
	Total	351	
TP	1.00	117	120.22
	2.00	117	200.37
	3.00	117	207.41
	Total	351	

Table 5. Mean Rank across phases: pre cyclone (phase 1), post cyclone (phase 2) and 20 days after Cyclone (DAC) (phase 3).

Phase - wise comparison of Available Phosphorus (AP)					
Sample 1-Sample 2	**Test Statistic**	**Std. Error**	**Std. Test Statistic**	**Sig.**	**Adj. Sig.[a]**
1.00–2.00	-3.821	13.266	−0.288	0.773	1.000
1.00–3.00	-31.782	13.266	-2.396	0.017	0.050
2.00–3.00	-27.962	13.266	-2.108	0.035	0.105

Table 6. Phase wise comparisons of the AP, pre cyclone (phase 1), post cyclone (phase 2) and 20th DAC (days after cyclone) (phase 3). Each row tests the null hypothesis that the Sample 1 and Sample 2 distributions are the same. Asymptotic significances (2-sided tests) are displayed. The significance level is 0.05. [a]Significance values have been adjusted by the Bonferroni correction for multiple tests.

Phase - wise comparison of Total Phosphorus (TP)					
Sample 1-Sample 2	**Test statistic**	**Std. error**	**Std. test statistic**	**Sig.**	**Adj. Sig.[a]**
1.00–2.00	-80.145	13.264	-6.043	0.000	0.000
1.00–3.00	-87.188	13.264	-6.574	0.000	0.000
2.00–3.00	-7.043	13.264	−0.531	0.595	1.000

Table 7. Phase wise comparisons of the TP, pre cyclone (phase 1), post cyclone (phase 2) and 20th DAC (days after cyclone) (phase 3). Each row tests the null hypothesis that the Sample 1 and Sample 2 distributions are the same. Asymptotic significances (2-sided tests) are displayed. The significance level is 0.05. a. Significance values have been adjusted by the Bonferroni correction for multiple tests.

yellow zone in the Banni grassland, which was the lowest, indicated that this area had the highest rate of dry dust deposition, with an average speed of approximately 6.09 m s^{-1}.

Correlation between aerosol scattering and dust deposition in Banni

The total number of metadata matrix calculations from the MERRA-2 model's data on total aerosol scattering (TAS) at 550 nm, dust wet deposition (DWD), and dust dry deposition (DDD) were used in the present study to examine the relationships between TAS, DWD, and DDD and determine their correlation with dust deposition. This research demonstrated that there was a negative correlation between TAS and DWD in the studied area. TAS and DDD did, however, show a positive correlation. In other words, an increase in the concentration of total aerosols has a positive impact on DDD. Using the Pearson correlation coefficient (r), the strength of the observed positive correlation and negative correlation between TAS and DWD and DDD was examined (Fig. 7). This correlation ranges from − 1 (perfectly representing a perfect negative correlation), 0 (representing no linear correlation), and + 1 (perfectly representing a perfect positive correlation). The average Pearson correlation

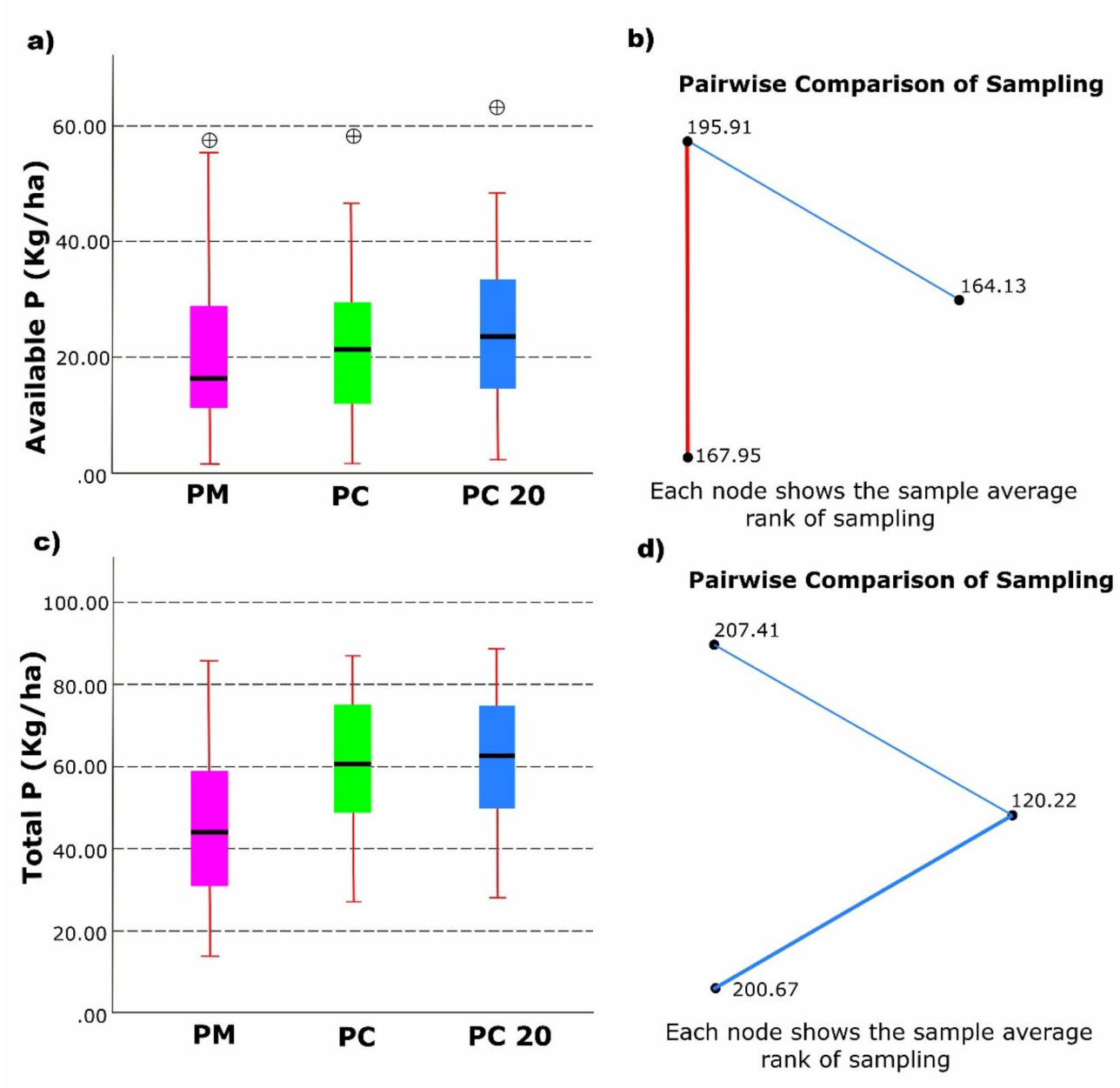

Fig. 3. Phase wise comparisons of the AP and TP, pre monsoon (PM), post cyclone (PC) and 20th DAC (PC 20). Outliers shown by circle with cross.

coefficient (r) between the TAS and the DWD was −0.74, demonstrating a negative correlation between them. However, the average Pearson correlation coefficient (r) between the TAS and DD was 0.78, demonstrating that there was a positive correlation between the two variables. TAS and DWD had a very good fitting negative correlation based on the coefficient of determination (R^2), whereas TAS and DDD had a positive relationship owing to the coefficient of determination (R^2). Variations in TAS values suggest that these variables directly influence whether DDD decreases or increases.

Impact of wind on aerosol scattering: insights from the wind rose plot and bubble plot analysis

The wind rose plot demonstrates the predominance of wind patterns from west to east, demonstrating the significant impact of marine air masses throughout the research period (Fig. 8).The predominant wind direction in the Banni grassland between 1981 and 2021, as shown by the statistical findings of wind direction and speed probability distribution in March-October, was a southwest wind. Compared to the usual wind direction from 1981 to 2021, the long-range transport of desert dust from western sources steadily increased the aerosol loading across the Banni Plain during these months on average. However, during the months of January, February, November and December, the region receives wind from the North, most likely from the Thar Desert region. The

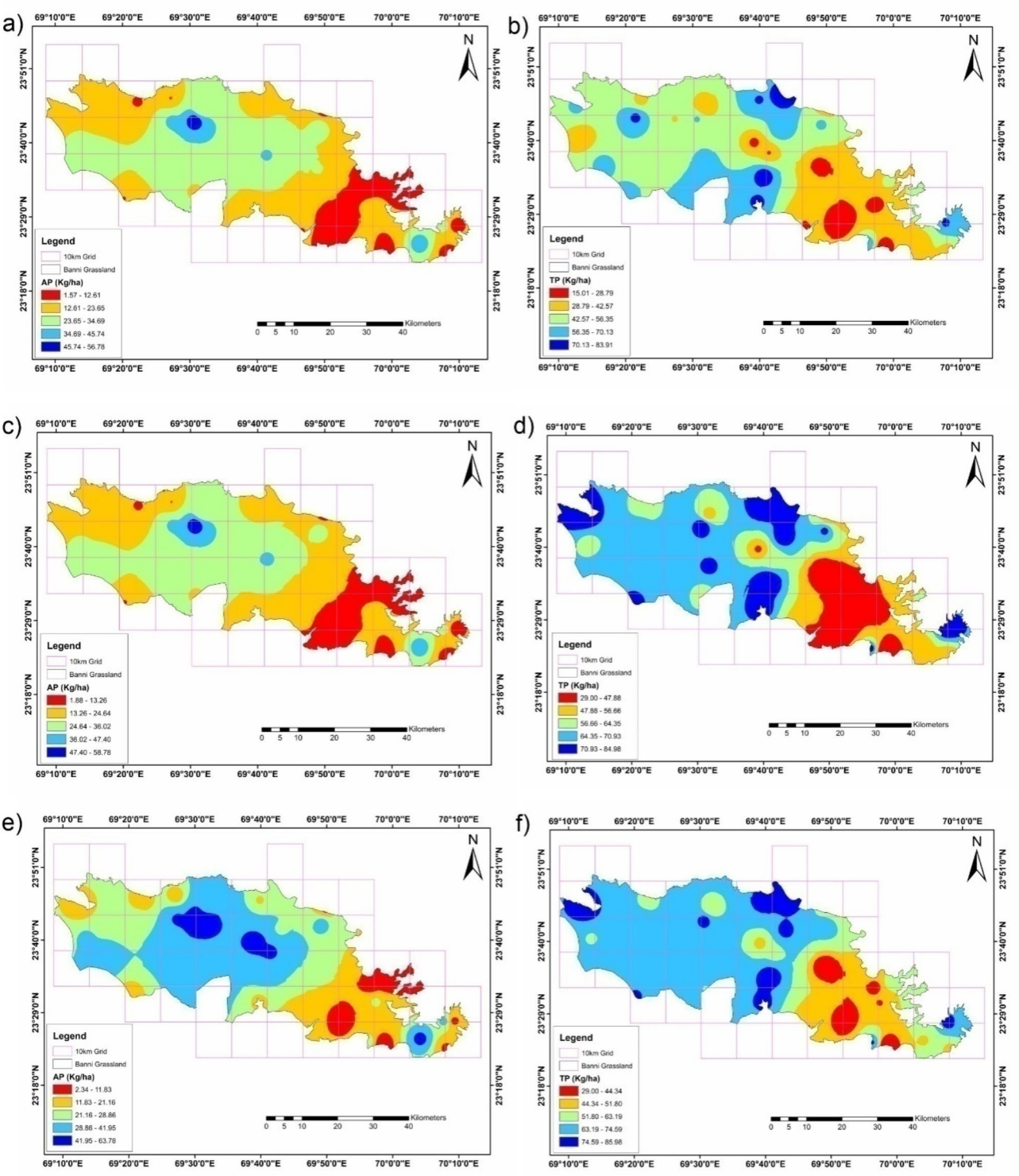

Fig. 4. Phasewise IDW spatial interpolation of AP and TP. (**a**) Premonsoon AP, (**b**) Pre monsoon TP, (**c**) postcyclone AP, (**d**) postcyclone TP, (**e**) 20 DAC AP and (**f**) 20 DAC TP. This map was created by the authors using ArcGIS software (version 10.7).

wind rose diagram for the entire study region also showed the dominance of the southwest flowing wind direction from March to October. During the months of June and July, the maximum wind speed across the region reaches approximately 8.5 m/s, whereas the minimum speed of 2.4 m/s is generally observed in the months of October and November. However, in the year 2023 (June), SW cyclonic winds mounted up to speeds ranging between 100 and 90 km/hr (Fig. 2). Figure 9 shows the monthly bubble plot from 1981 to 2021 with respect to total aerosol scattering. Figure 9a, b,k and l shows that the total aerosol scattering is mainly concentrated in the 0°–

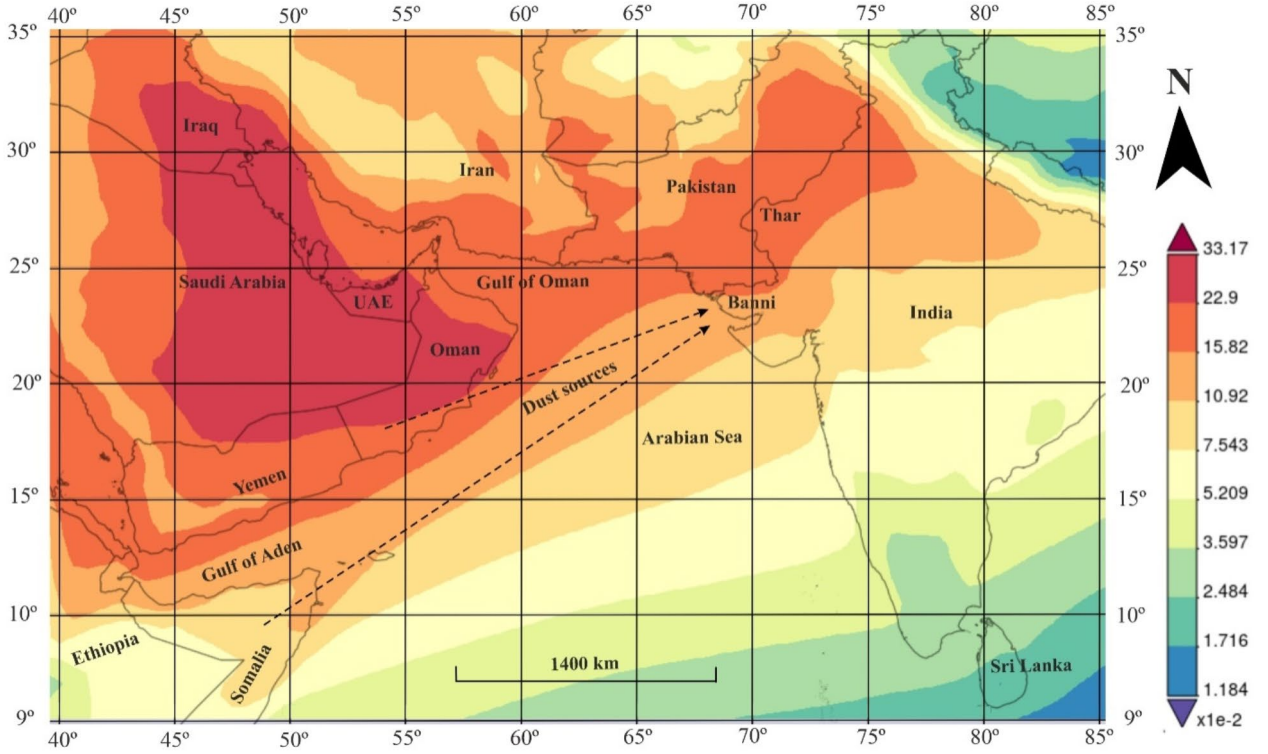

Fig. 5. Time-averaged map of Dust scattering AOT 550 nm monthly 0.5 * 0.625 degree (MERRA-2) from 1981 January to 2021 December. The locations of major sources of dust storms over the Indian subcontinent are marked by arrows striking SW of the Banni Grassland. This map was created by the authors from Earth data (https://giovanni.gsfc.nasa.gov/giovanni/) and ArcGIS software (version 10.7).

50° and 300°-350° wind directions; that is, the total aerosol concentration in January, February, November and Decembermainly occurs from winds blowing from the northern direction (Thar Desert), and the total aerosol scattering mostly occurs in the period when the wind speed is less than or equal to 4 m/s. Figure 9c, d,e, f,g, g, h, and l shows that the total aerosol scattering is mainly concentrated in the 225°-290° wind direction; that is, the total aerosol concentration in March, April, May, June, July, August, and September is mainly caused by winds blowing from the south west and west (MENA) direction, and the total aerosol scattering is mostly caused by winds less than or equal to 7.5 m/s. However, total aerosol concentrations were observed in the range of 250°-350° in the wind direction (west and northwest) in October (Fig. 9j), and scattering occurred mostly in that month when the wind speed was less than or equal to 3.4 m/s.

The pre- and post-cyclonic data for the TP are consistent with the fact that wet deposition by aerosols during this postcyclonic phase led to an increase in the TP content in the soil ($p \leq 0.05$). However, there was no significant change in the TP post-20 DAC ($p > 0.05$). As far as AP is concerned, the pre- and post-cyclonic data were not significantly different ($p > 0.05$). However, pre- and post-cyclonic data for AP were much less than those for 20 DAC, which is attributable to the microbial load that might have increased from cyclonic aerosol movement and hence the conversion of AP to TP (Fig. 10). The present study planned period of 1981–2021 was in accordance with the data availability frame period from MERRA-2. However, the cyclonic event on June 16 originating from the Arabian Sea with the same wind pattern helped us confirm our findings for the above period.

Conclusion

Investigating how environmental conditions impact the functioning of different grasslands in the context of climate change is therefore crucial.Savannahs, other dryland ecosystems, and tropical and subtropical grasslands cover a large portion of the globe and are vital for sustaining human lifestyles.It is also well acknowledged that phosphorus is a limiting factor for terrestrial ecosystem production.The primary productivity, nutrient availability, and plant community structure of grassland ecosystems are influenced by the phosphorus (P) cycle. Owing to its poor solubility and fixation into locked forms in soil, P has played a limiting role in ecosystems. In the past several centuries, regional processes, including weathering of parent materials, breakdown of organic matter, and biological fixation, have been attributed to the sources of phosphorus in grasslands. However, recent studies have emphasised the importance of long-distance air transport in supplying distant ecosystems with external nutrient inputs.

The present study is the first attempt to understand P transformations in grassland ecosystems via aerosol movement driven by wind patterns and cyclonic influences. This major attempt to harness the power of the atmospheric movement of aerosols in altering P levels in soils calls for further studies in ecosystems where P

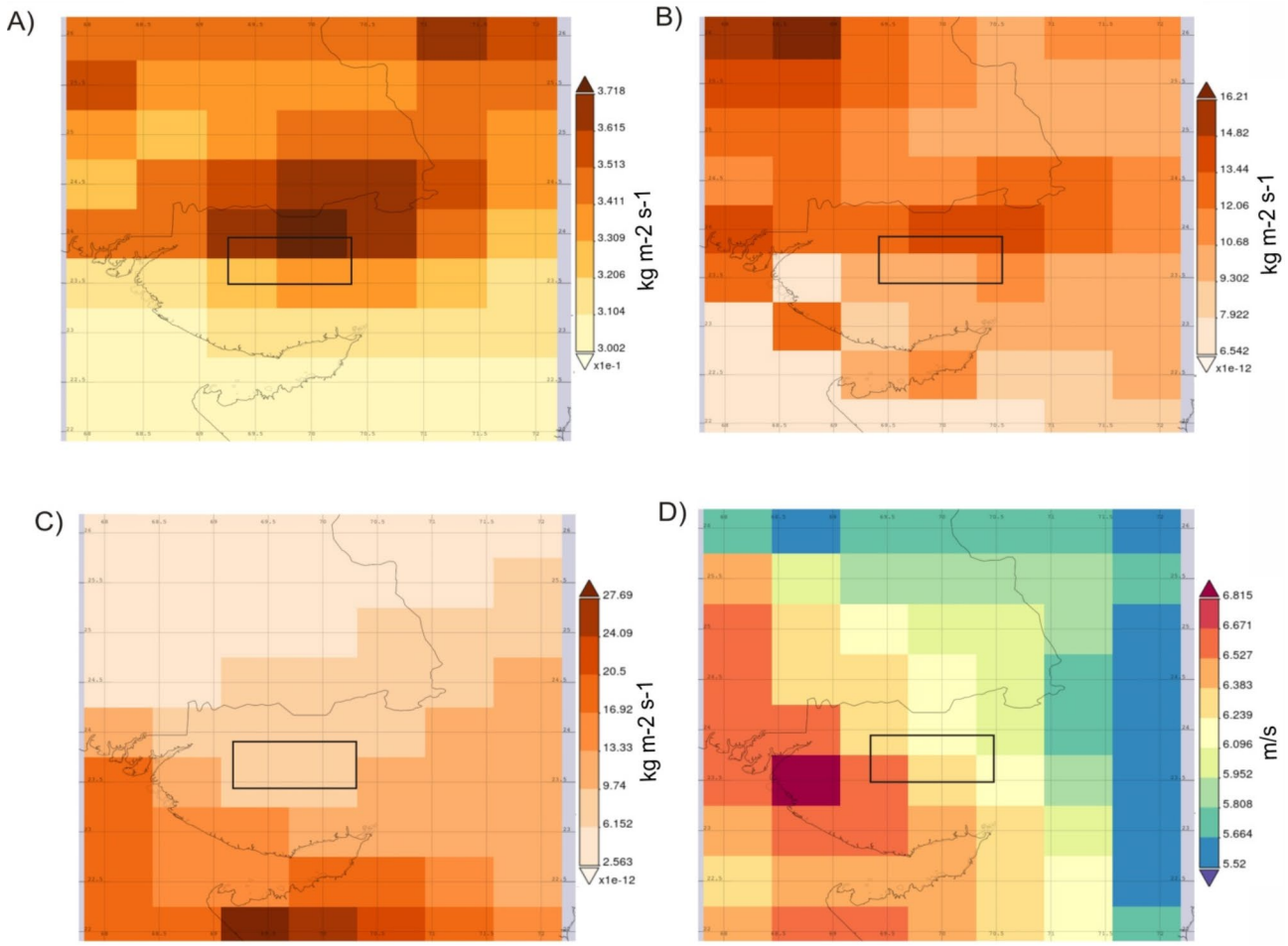

Fig. 6. (**A**) Spatial time average map of total aerosol scattering (TAS) at 550 nm monthly (unit less) over the Banni grassland and surrounding regions derived from the MERRA-2 model during the period 1981–2021. The black box indicates the location of the Banni grassland. (**B**) MERRA-2 model-derived spatial time average map of monthly dust dry deposition (kg m^{-2} s^{-1}) over the Banni grassland from 1981 to 2021. (**C**) MERRA-2 model-derived spatial time average map of dust wet deposition monthly (kg m^{-2} s^{-1}) over the Banni grassland from 1981 to 2021. (**D**) Wind speed monthly (m/s) spatial time average map over the Banni grassland from 1981 to 2021 generated from the MERRA-2 model. This map was created by the authors from Earth data (https://giovanni.gsfc.nasa.gov/giovanni/) and ArcGIS software (version 10.7).

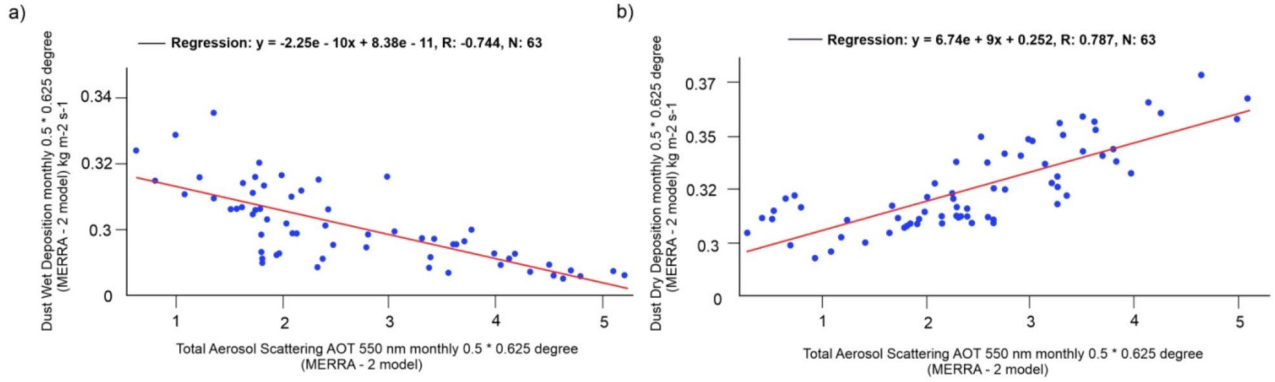

Fig. 7. Correlation coefficients between TAS and DWD and DDD from 1981 to 2021. (**a**) Correlation between DWD and TAS and (**b**) Correlation between DDD and TAS. This graph was created by the authors using Origin Pro 2022 (https://www.originlab.com/2022).

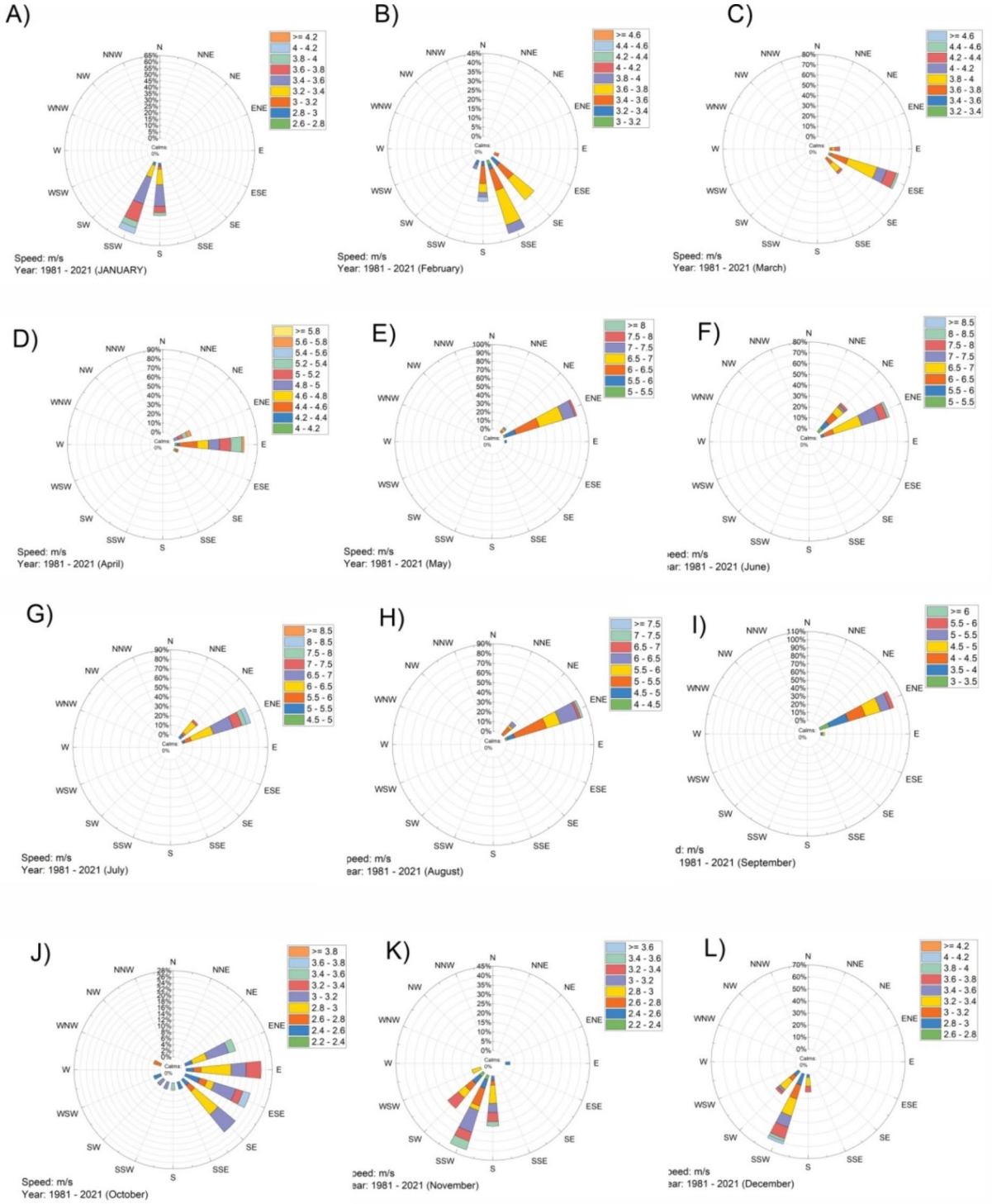

Fig. 8. Wind rose plot showing the wind direction and distribution of wind speed (m/s) across the study site (Banni grassland) from 1981 to 2021 for (**A**) January, (**B**) February, (**C**) March, (**D**) April, (**E**) May, (**F**) June, (**G**) July, (**H**) August, (**I**) September, (**J**) October, (**K**) November, and (**L**) December. The diameter of the bubble plot represents the intensity of total aerosol scattering, irrespective of the colour code.

levels have shown compromised differences in vegetation dynamics. Grassland ecosystems are very fragile and sensitive to the influence of nutrients. Owing to its unique fixation properties, phosphorus, which is a crucial and limiting nutrient, requires the strategic input of a microbial load (inherent source or external input), as in the chemistry of P transition, the conversion from one form to another plays an important role.The role of

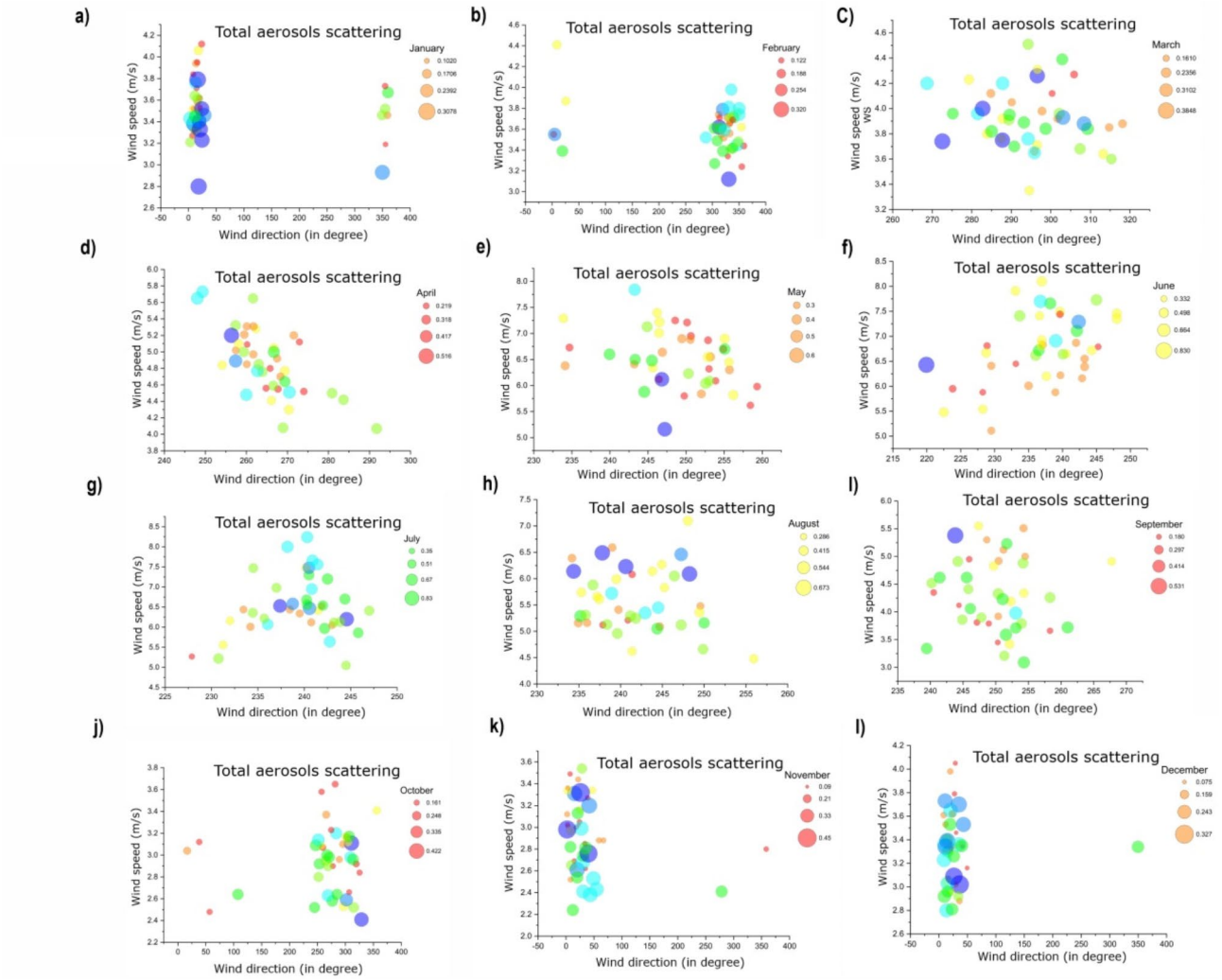

Fig. 9. Bubble plot showing total aerosol scattering with respect to wind direction and wind speed (m/s) across the study site (Banni grassland) from 1981 to 2021 on (**A**) January, (**B**) February, (**C**) March, (**D**) April, (**E**) May, (**F**) June, (**G**) July, (**H**) August, (**I**) September, (**J**) October, (**K**) November, and (**L**) December.

PSM in conversion of locked P forms to bioavailable forms has been well established in previous studies. This maiden attempt to understand this conversion under the influence of a cyclonic event that leads to conducive environment for PSM growth is well shown through data. The cyclonic circulation during the study period altered the aerosol depositional pattern, which agreed with our ground data for phosphorus. In the present study, we investigated the role of MENA and Thar Desert dust storms as precursors of P deposition patterns in the Asiatic grasslands of western India. The cyclonic influence on aerosol movement has been identified as a possible game changer in the P dynamics of grassland ecosystems. The findings of our study suggest that wet deposition by aerosols, specifically during post cyclonic phases, leads to increased P content in soils, potentially altering vegetation dynamics. The limited knowledge on the aeolian movement of P, specifically in unique grassland ecosystems, could pave the way for sustainable management of this fragile ecosystem.

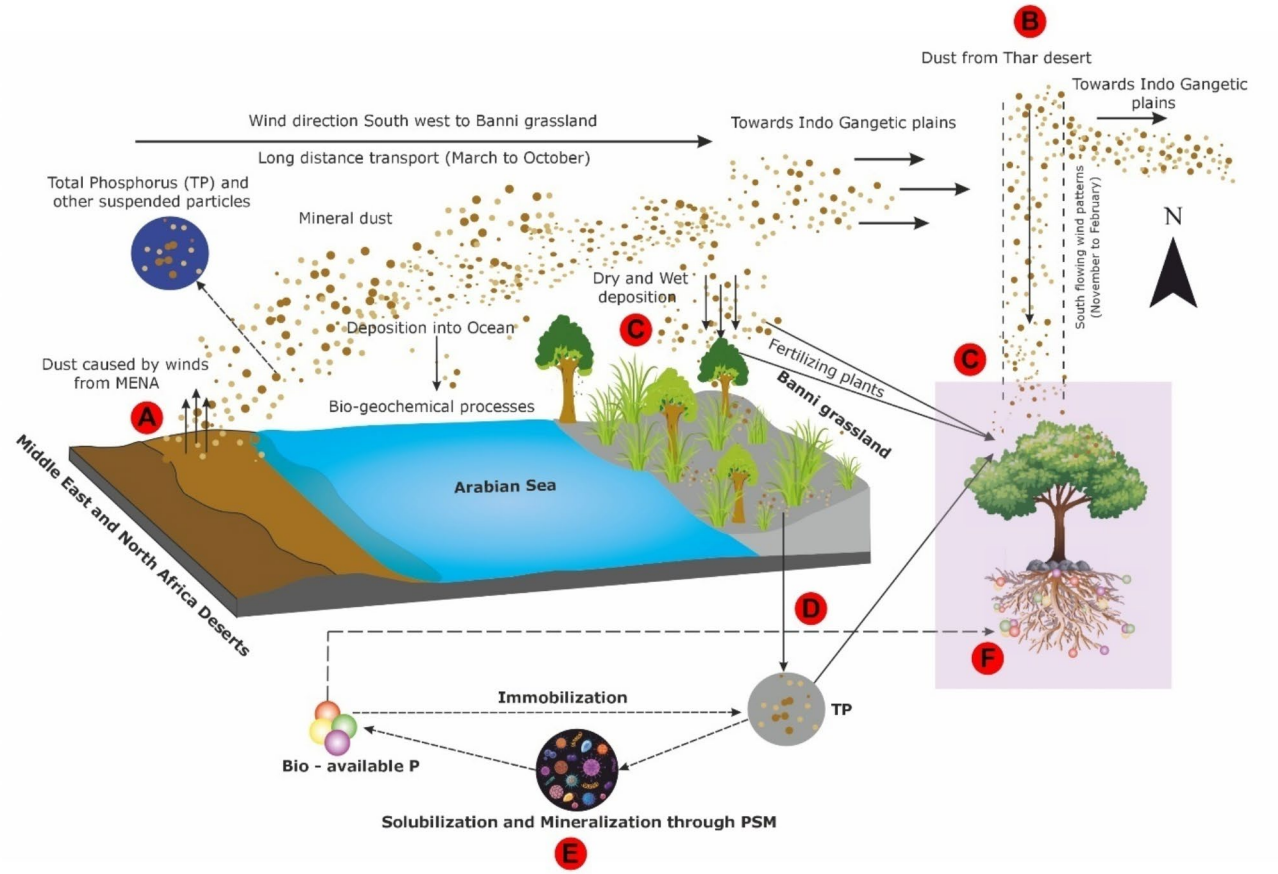

Fig. 10. The diagram illustrates (not to scale) the journey of mineral dust, total phosphorus (TP), and other suspended particles originating from the Middle East and North Africa (MENA) deserts and the Thar desert, and their impact on the Banni grassland. (**A**) Dust Sources and Transport: Dust from MENA deserts is mobilized by winds and transported long distances towards the Banni grassland from March to October, as depicted by the arrows moving from MENA. (**B**) Simultaneously, dust from the Thar desert is carried southwards towards the Indo-Gangetic plains from November to February. (**C**) Deposition: Long-distance transport of dust, which includes phosphorus, travels from these arid and semi-arid regions (MENA and Thar) across the Arabian Sea, eventually settling on the Banni grassland through wet and dry deposition, fertilizing grassland by introducing new nutrient sources. (**D**) Biogeochemical Processes: Within the Banni grassland, the deposition of mineral dust and TP leads to the immobilization of phosphorus. (**E**) Phosphate-solubilizing microorganisms (PSM) play a crucial role in solubilizing and mineralizing TP, transforming it into bio-available phosphorus (Bio-available P) which is essential for plant nutrition. The diagram also shows how events like Cyclone Biparjoy contribute to the transport of dust over the Arabian Sea, affecting soil phosphorus availability and triggering changes in phosphorus activation coefficients (PAC), essential for the productivity of grasses and plants. (**F**) Ecological impact: The bio-available P enhances the fertilization of plants in the Banni grassland, promoting vegetation growth and ecological balance. The illustration highlights the interconnected nature of dust transport, deposition, and nutrient cycling between arid regions, marine environments, and terrestrial ecosystems.

Data availability

Data is provided within the manuscript.

Received: 6 November 2024; Accepted: 25 December 2024
Published online: 05 February 2025

References

1. Suttie, J. M., Reynolds, S. G. & Batello, C. *Grasslands of the World*vol. 34 (Food & Agriculture Org, 2005).
2. Byrnes, R. C., Eastburn, D. J., Tate, K. W. & Roche, L. M. A global meta-analysis of grazing impacts on soil health indicators. *J. Environ. Qual.* **47**, 758–765 (2018).
3. Wang, N. et al. Effects of climate warming on carbon fluxes in grasslands—a global meta-analysis. *Glob Chang. Biol.* **25**, 1839–1851 (2019).

4. Huber, R., Le'Clec'h, S., Buchmann, N. & Finger, R. Economic value of three grassland ecosystem services when managed at the regional and farm scale. *Sci. Rep.* **12**, 4194 (2022).
5. Bardgett, R. D. et al. Combatting global grassland degradation. *Nat. Rev. Earth Environ.* **2**, 720–735 (2021).
6. Lorenz, K., Lal, R., Lorenz, K. & Lal, R. Carbon sequestration in grassland soils. *Carbon Sequestration Agric. Ecosyst.* 175–209 (2018).
7. Sarmiento, G., Da Silva, M. P., Naranjo, M. E. & Pinillos, M. Nitrogen and phosphorus as limiting factors for growth and primary production in a flooded savanna in the Venezuelan Llanos. *J. Trop. Ecol.* **22**, 203–212 (2006).
8. Niinemets, Ü. & Kull, K. Co-limitation of plant primary productivity by nitrogen and phosphorus in a species-rich wooded meadow on calcareous soils. *Acta Oecol.* **28**, 345–356 (2005).
9. Harpole, W. S. et al. Addition of multiple limiting resources reduces grassland diversity. *Nature* **537**, 93–96 (2016).
10. Fay, P. A. et al. Grassland productivity limited by multiple nutrients. *Nat. Plants*. **1**, 1–5 (2015).
11. Luo, R. et al. Nitrogen and phosphorus enrichment accelerates soil organic carbon loss in alpine grassland on the Qinghai-Tibetan Plateau. *Sci. Total Environ.* **650**, 303–312 (2019).
12. Violaki, K. et al. Bioaerosols and dust are the dominant sources of organic P in atmospheric particles. *Npj Clim. Atmos. Sci.* **4**, (2021).
13. Dey, R., Sharma, S. B. & Thakkar, M. G. Livestock movement driven phosphorus transitions as core drivers of grassland vegetation dynamics. *Catena* **235**, 107694 (2024).
14. Yang, X., Post, W. M., Thornton, P. E. & Jain, A. The distribution of soil phosphorus for global biogeochemical modeling. *Biogeosciences* **10**, 2525–2537 (2013).
15. Mahowald, N. et al. Global distribution of atmospheric phosphorus sources, concentrations and deposition rates, and anthropogenic impacts. *Global Biogeochem. Cycles* **22**, (2008).
16. Okin, G. S., Mahowald, N., Chadwick, O. A. & Artaxo, P. Impact of desert dust on the biogeochemistry of phosphorus in terrestrial ecosystems. *Global Biogeochem.* **Cycles18**, (2004).
17. Bayon, G. et al. Contribution of Saharan dust to chemical weathering fluxes and associated phosphate release in West Africa. *Earth Planet. Sci. Lett.* **641**, 118845 (2024).
18. Prospero, J. M. et al. Characterizing and quantifying African dust transport and deposition to South America: Implications for the phosphorus budget in the Amazon Basin. *Global Biogeochem. Cycles*34, eGB006536 (2020). (2020).
19. Griffin, D. W. & Kellogg, C. A. Dust storms and their impact on ocean and human health: Dust in Earth's atmosphere. *Ecohealth*1, 284–295 (2004).
20. Graham, W. F. & Duce, R. A. Atmospheric pathways of the phosphorus cycle. *Geochim. Cosmochim. Acta*. **43**, 1195–1208 (1979).
21. Meng, Y. et al. The sources and atmospheric pathway of phosphorus to a high alpine forest in eastern Tibetan Plateau, China. *J. Geophys. Res. Atmos.*125, eJD031327 (2020).
22. Mahowald, N. et al. Aerosol impacts on climate and biogeochemistry. *Annu. Rev. Environ. Resour.* **36**, 45–74 (2011).
23. Tipping, E. et al. Atmospheric deposition of phosphorus to land and freshwater. *Environ. Sci. Process. Impacts*. **16**, 1608–1617 (2014).
24. Anderson, L. D., Faul, K. L. & Paytan, A. Phosphorus associations in aerosols: What can they tell us about P bioavailability? *Mar. Chem.* **120**, 44–56 (2010).
25. Diao, X. et al. Atmospheric phosphorus and its geochemical cycling: Fundamentals, progress, and perspectives. *Earth Sci. Rev.* 104492 (2023).
26. Sharma, S. B. & Chowdhury, A. Phosphorus transitions in traditional eco-knowledge versus chemical based agri-amendment systems of stress-prone semi-arid tropics: finding the real game-changer. *Ecol. Indic.* **121**, 107145 (2021).
27. Ziadi, N., Whalen, J. K., Messiga, A. J. & Morel, C. Assessment and modeling of soil available phosphorus in sustainable cropping systems. *Adv. Agron.* **122**, 85–126 (2013).
28. Sharma, S. B., Sayyed, R. Z., Trivedi, M. H. & Gobi, T. A. Phosphate solubilizing microbes: Sustainable approach for managing phosphorus deficiency in agricultural soils. *Springerplus*2, 1–14 (2013).
29. Ali, S., Zahid, A., Ahmed, M. U., Liaqat, I. & Aftab, M. N. Properties of aerosol particles in the air and their effects on greenhouse gases dispersion. in *Adv. Technol. Dev. Greenh. Gases: Emission Capture Convers.* 71–102 (Elsevier, 2024).
30. Vet, R. et al. A global assessment of precipitation chemistry and deposition of sulfur, nitrogen, sea salt, base cations, organic acids, acidity and pH, and phosphorus. *Atmos. Environ.* **93**, 3–100 (2014).
31. Wang, R. et al. Significant contribution of combustion-related emissions to the atmospheric phosphorus budget. *Nat. Geosci.* **8**, 48–54 (2015).
32. Nogueira, J. et al. Dust arriving in the Amazon basin over the past 7,500 years came from diverse sources. *Commun. Earth Environ.* **2**, 1–11 (2021).
33. Wang, X. et al. Dust deposition and its significance to soil nutrients in the Otindag Desert, China. *J. Arid Environ.* **194**, 104612 (2021).
34. Katra, I. et al. Substantial dust loss of bioavailable phosphorus from agricultural soils. *Sci. Rep.* **6**, 24736 (2016).
35. Aciego, S. M. et al. Dust outpaces bedrock in nutrient supply to montane forest ecosystems. *Nat. Commun.* **8**, 14800 (2017).
36. Gu, C. et al. Aeolian dust deposition and the perturbation of phosphorus transformations during long-term ecosystem development in a cool, semi-arid environment. *Geochim. Cosmochim. Acta*. **246**, 498–514 (2019).
37. Bauters, M. et al. Fire-derived phosphorus fertilization of African tropical forests. *Nat. Commun.* **12**, 5129 (2021).
38. Lequy, É., Conil, S. & Turpault, M. P. Impacts of aeolian dust deposition on European forest sustainability: A review. *Ecol. Manage.* **267**, 240–252 (2012).
39. Weathers, K. C. & Ponette-González, A. G. Atmospheric Deposition. in *Forest Hydrology and Biogeochemistry: Synthesis of past Research and Future Directions*. 357–370 (Springer, (2011).
40. Redfield, G. W. Atmospheric deposition of phosphorus to the Everglades: Concepts, constraints, and published deposition rates for ecosystem management. *Sci. World J.* **2**, 1843–1873 (2002).
41. Knippertz, P. & Stuut, J. B. W. Mineral dust. *Min. dust—A key Play. Earth Syst.* 121–147 (2014).
42. Kurosaki, Y., Kinugasa, T., Nyamtseren, M., Liu, S. & Otani, S. Impacts of aeolian desertification and dust storms on ecosystems, economic development, and human health. in *Combating Aeolian Desertification in Northeast Asia* 129–158 (Springer, 2022).
43. Darvishi Boloorani, A. et al. Springer,. Sources, drivers, and impacts of sand and dust storms: a global view. in *Dust and Health: Challenges and Solutions* 31–49 (2023).
44. Maji, S. & Sonwani, S. Nature of Sand and Dust Storm in South Asian Region: extremities and environmental impacts. in *Extremes in Atmospheric Processes and Phenomenon: Assessment, Impacts and Mitigation*. 113–139 (Springer, (2022).
45. Choobari, O. A., Zawar-Reza, P. & Sturman, A. The global distribution of mineral dust and its impacts on the climate system: A review. *Atmos. Res.* **138**, 152–165 (2014).
46. Xiong, J. et al. Climate characteristics of dust aerosol and its transport in major global dust source regions. *J. Atmos. Solar Terr. Phys.* **209**, 105415 (2020).
47. Awadh, S. M. Impact of north African sand and dust storms on the Middle East using Iraq as an example: Causes, sources, and mitigation. *Atmos. (Basel).* **14**, 180 (2023).
48. Sivakumar, M. V. K. Impacts of sand storms/dust storms on agriculture. in *Natural Disasters and Extreme Events in Agriculture: Impacts and Mitigation* 159–177 (Springer, 2005).

49. Rabbani, F. & Sharifikia, M. Prediction of sand and dust storms in West Asia under climate change scenario (RCPs). *Theor. Appl. Climatol.* **151**, 553–566 (2023).
50. Hamzeh, N. H., Karami, S., Opp, C., Fattahi, E. & Jean-François, V. Spatial and temporal variability in dust storms in the Middle East, 2002–2018: Three case studies in July 2009. *Arab. J. Geosci.* **14**, 538 (2021).
51. Shaheen, A. et al. Spatio-temporal changes of spring-summer dust AOD over the eastern mediterranean and the middle east: Reversal of dust trends and associated meteorological effects. *Atmos. Res.* **281**, 106509 (2023).
52. Khakifirouz, Z., Niknami, M., Keshavarz, M. & Sabouri, M. S. Transition from vulnerability to resilience to dust storms: A mixed-methods research. *Nat. Hazards* 1–22 (2024).
53. Singh, R. P., Dey, S., Tripathi, S. N., Tare, V. & Holben, B. Variability of aerosol parameters over Kanpur, northern India. *J. Geophys. Res. D Atmos.* **109**, 1–14 (2004).
54. Kayetha, V. K., Senthilkumar, J., Prasad, A. K., Cervone, G. & Singh, R. P. Effect of dust storm on ocean color and snow parameters. *J. Indian Soc. Remote Sens.* **35**, 1–9 (2007).
55. Prasad, A. K. & Singh, R. P. Changes in aerosol parameters during major dust storm events (2001–2005) over the Indo-Gangetic Plains using AERONET and MODIS data. *J. Geophys. Res. Atmos.* **112**, (2007).
56. Rajesh, P. V. & Goswami, B. N. Climate change and potential demise of the Indian deserts. *Earth's Futur.*11, eEF003459 (2023).
57. Ramachandran, S. & Cherian, R. Regional and seasonal variations in aerosol optical characteristics and their frequency distributions over India during 2001–2005. *J. Geophys. Res. Atmos.* **113**, 1–16 (2008).
58. Arora, A. S. & Reddy, A. S. Development of multiple linear regression models for predicting the stormwater quality of urban sub-watersheds. *Bull. Environ. Contam. Toxicol.* **92**, 36–43 (2014).
59. Reuter, M., Piller, W. E., Harzhauser, M. & Kroh, A. Cyclone trends constrain monsoon variability during late Oligocene sea level highstands (Kachchh Basin, NW India). *Clim. Past.* **9**, 2101–2115 (2013).
60. Evan, A. T. & Camargo, S. J. A climatology of Arabian Sea cyclonic storms. *J. Clim.* **24**, 140–158 (2011).
61. Nigam, R. & Chaturvedi, S. K. Do inverted depositional sequences and allochthonous foraminifers in sediments along the Coast of Kachchh, NW India, indicate palaeostorm and/or tsunami effects? *Geo-Mar. Lett.* **26**, 42–50 (2006).
62. Evan, A. T., Kossin, J. P., 'Eddy'Chung, C. & Ramanathan, V. Arabian Sea tropical cyclones intensified by emissions of black carbon and other aerosols. *Nature* **479**, 94–97 (2011).
63. Wu, Q. et al. Characterizing differences in the phosphorus activation coefficient of three typical cropland soils and the influencing factors under long-term fertilization. *PLoS One.* **12**, e0176437 (2017).
64. Pastoral, S. Let it be Banni Understanding and Sustaining Pastoral Livelihoods of Banni. (2012).
65. Kumar, A., Mahato, R. & Gajera, N. Distribution pattern of birds in Banni Grassland of Kachchh district, Gujarat, India. (2014).
66. Rawat, G. S. & Adhikari, B. S. (eds). *Ecology and Management of Grassland Habitats in India, ENVIS Bulletin. Wildlife and Protected Areas.* vol. 17 (2015).
67. Kar, A. Characteristics of major soils of Banni mudflat in arid western India and their relationship with topography. (2001). https://doi.org/10.1006/jare.2000.0765
68. Kumar, A. & Mahato, R. Ecology and Management of Banni Grassland of Kachchh, Gujarat. *Ecol. Manag Grassl Habitats India* **240** (2015).
69. Biswas, S. K. Mesozoic and Tertiary Stratigraphy of Kutch*(Kachchh)—A Review. in *Conference GSI* 1–24 (2016).
70. Biswas, S. K. Landscape of Kutch—a morphotectonic analysis. *Indian J. Earth Sci.* **1**, 177–190 (1974).
71. Biswas, S. K. Regional tectonic framework, structure and evolution of the western marginal basins of India. *Tectonophysics*135, 307–327 (1987).
72. Alef, K. & Nannipieri, P. *Methods in Applied Soil Microbiology and Biochemistry* (Academic, 1995).
73. Olsen, S. R. *Estimation of Available Phosphorus in Soils by Extraction with Sodium Bicarbonate* (US Department of Agriculture, 1954).
74. Bowman, R. A. A rapid method to determine total phosphorus in soils. *Soil. Sci. Soc. Am. J.* **52**, 1301–1304 (1988).
75. Walkley, A. & Black, I. A. An examination of the Degtjareff method for determining soil organic matter, and a proposed modification of the chromic acid titration method. *Soil. Sci.* **37**, 29–38 (1934).

Acknowledgements
NA.

Author contributions
R.D. and S.B.S. analysed and interpreted the data. R.D. and S.B.S. framed the manuscript. R.D. prepared the maps. M.G.T., R.K.S., A.C. and A.N. refined the manuscript. All authors read and approved the final manuscript.

Funding
The authors express their sincere gratitude to the anonymous reviewers and the editor for their invaluable comments and suggestions, which greatly contributed to improving the quality of this paper. Special thanks are extended to the Education Department, Government of Gujarat, for providing the SHODH Fellowship to Rupak Dey, enabling him to pursue his Ph.D. research work. This paper forms a part of the Doctoral Thesis of Mr. Rupak Dey.

Declarations

Competing interests
The authors declare no competing interests.

Additional information
Correspondence and requests for materials should be addressed to R.D. or S.B.S.

Reprints and permissions information is available at www.nature.com/reprints.

Publisher's note Springer Nature remains neutral with regard to jurisdictional claims in published maps and institutional affiliations.